Monte Carlo Characterization of Short-Wave Infrared Optical Wavelengths for Biosensing Applications

K. Budidha, S. Chatterjee, M. Qassem, and P. A. Kyriacou, *Senior Member, IEEE*

***Abstract*— Short-wave infrared (SWIR) spectroscopy has shown great promise in probing the composition of biological tissues. Currently there exists an enormous drive amongst researchers to design and develop SWIR-based optical sensors that can predict the concentration of various biomarkers non-invasively. However, there is limited knowledge regarding the interaction of SWIR light with vascular tissue, especially in terms of parameters like the optimal source-detector separation, light penetration depth, optical pathlength, etc., all of which are essential components in designing optical sensors. With the aim to determine these parameters, Monte Carlo simulations were carried out to examine the interaction of SWIR light with vascular skin. SWIR photons were found to penetrated only 1.3 mm into the hypodermal fat layer. The highest optical pathlength and penetration depths were seen at 1mm source-detector separation, and the lowest being 0.7mm. Although the optical pathlength varied significantly with increasing source-detector separation at SWIR wavelengths, penetration depth remained constant. This may explain why collecting optical spectra from depth of tissue at SWIR wavelengths is more challenging than collecting optical spectra from near-infrared wavelengths, where both the optical pathlength and penetration depth change rapidly with source-detector separation.**

I. Introduction

Short-Wave Infrared (SWIR) spectroscopy is the transmission of infrared light (commonly between ~ 1200 nm to 2500 nm) into a biological tissue sample and the identification of diffusely reflected light from the sample to interrogate the tissue composition, structure and function. When compared to visible or near infrared spectroscopy (400 to 1000 nm), SWIR spectroscopy has shown to have increased photothermal sensitivity to chromophores within tissue such as water (near 1150, 1450, and 1900 nm), lipids (near 1040, 1200, 1400, and 1700 nm), and collagen (between 1200 and 1500 nm) [1]. Given this advantage, researchers have attempted to use the SWIR region to characterize essential biomarkers such as glucose, lactate, ethanol, uric acid, and others in a non-invasive manner. However, due to the high absorption of water in this region, direct quantification of these biomarkers has not been possible. Nonetheless, with machine learning tools becoming more mainstream, researchers have sorted to using these multivariate regression methods to analyze and quantify biomarker concentrations from the *in vivo* SWIR spectra. Some of the recent work in this area include [2]-[5]. These preliminary *in vitro* and *in vivo* investigations have shown great promise and have paved the way for the development of novel optical sensors that can measure a variety of biomarkers non-invasively.

None of these investigations, however, have focused on determining the type of interactions that take place between vascular tissue and SWIR light, which is critical in evaluating the sensor's effectiveness for biomarker assessment. The applicability of any optical sensor for biomarker assessment largely depends on the anatomy of the tissue region-of-interest (ROI), the design of the sensor (e.g., wavelength, shape and size of the optical source and detector, source-detector separations, etc.) and the optical interactions between the optical sensor and vascular tissue (penetration depth of light at a given wavelength, optical pathlength, etc.); such crucial details have so far never been considered and investigated.

Hence, to understand the interaction of SWIR light with vascular tissues, and to determine the sensor design characteristics that are required when applying SWIR spectroscopy, we aim to create a robust in-silico model based on the Monte Carlo (MC) method. MC is the most reliable computational approach for simulating light-tissue interactions. MC method has been adapted and appreciated by researchers for solving critical tissue-optics related problems for many years [2]-[10]. In the current paper, a detailed Monte Carlo model of human skin has been explored for characterizing the optical path through tissue at the SWIR optical wavelengths. Variables, which are essential in the optimization of optical sensor design, such as light-tissue interaction profile, optical pathlength and penetration depths have been investigated in this study and preliminary results are presented.

II. Methodology

In a Monte Carlo (MC) optical model, virtual photon packets are simulated as they pass through a volume of tissue which is a highly scattering and partly absorbing medium. The medium is characterized by its wavelength-dependent optical properties, e.g., scattering coefficient (μ_s), absorption coefficient (μ_a) and scattering anisotropy (g).

In this work, the MC model was designed in MATLAB® (Mathworks, Inc., USA). The virtual photons were launched randomly into the tissue surface, following a Gaussian beam profile. The optical path of the photon packet was simulated by tracing the photon's steps through the medium, determined by random sampling of the probability distribution p(s) for the photon's free pathlength

K Budidha, S. Chatterjee, M. Qassem, and P. A. Kyriacou, are with the Research Centre for Biomedical Engineering at City, University of London, Northampton Square, London, EC1V 0HB (phone: 020-7040-3878; e-mail: karthik.budidha.1@city.ac.uk).

s between two consecutive interaction events as shown in Eq. 1:

$$p(s) = \mu_s e^{-\mu_s . s} \qquad \ldots\ldots (1)$$

The step size s of a photon packet was calculated as:

$$s = -\frac{\ln(\xi)}{\mu_s} \qquad \ldots\ldots (2)$$

where ξ is a computer-generated pseudo random number lying between 0 and 1. Once the step-size was determined, scattering was achieved by orienting the photon's direction through two randomly generated angles zenith (θ) and azimuth (ϕ), described respectively in Eqs. 3 and 4.

$$\cos\theta = \frac{1}{2g}\left[1 + g^2 - \left(\frac{1 - g^2}{1 - g + 2g\xi}\right)\right] \ldots\ldots (3)$$

$$\phi = 2\pi\xi \qquad \ldots\ldots (4)$$

Each of the launched photon packets was introduced with an initial statistical weight w=1. After each step size, when the photon packet reached an interaction site, a fraction of its weight ($w.\frac{\mu_a}{\mu_a+\mu_s}$) was modelled to be absorbed within the tissue-layer. The Russian roulette technique was used for the termination of the photon packets within the medium, weighing below a threshold weight $w_{th} = 10^{-4}$. If the photon packet was exiting the tissue surface, the fulfilment of the detection criteria was tested (i.e., if the photon had reached the circular area of the detector), with the undetected photons leaving the tissue surface being discarded. The photon path was traced within the tissue layers until it was detected, discarded, or terminated. The corrections due to reflection and refraction were considered each time the photon hit the boundary. The number of photons detected for the range of source-detector separations was 10^{10}.

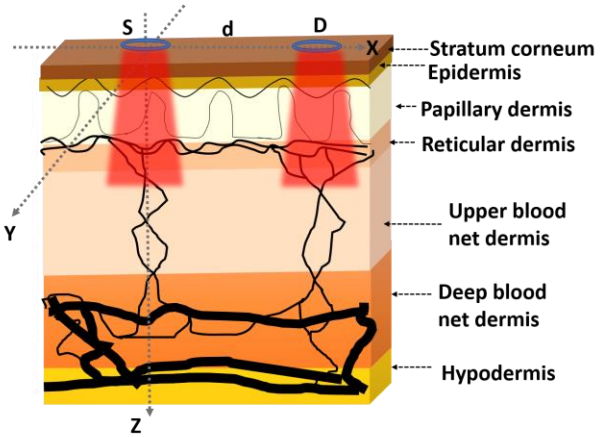

Fig.1. Monte Carlo simulation setup. The skin tissue volume is presented in a 3D Cartesian co-ordinate where the optical source S is placed on the origin of the system and the detector is placed at a distance d from the source.

Simulated skin tissue volume had a semi-infinite length and a thickness of 1.5mm thick and was composed of stratum corneum (0.02mm thick), epidermis (0.25mm thick), dermis (0.68mm thick) and hypodermal fat (0.55mm thick). The two outermost skin layers, i.e., stratum corneum and epidermis, were bloodless; and respectively 5% and 20% of those tissue volumes consisted of water (including blood plasma). Dermis was divided into four sublayers depending on the different distributions in blood content at different depths: papillary dermis (0.1 mm thick, 4% blood, 50% water), upper blood net dermis (0.08 mm thick, 30% blood, 60% water), reticular dermis (0.2 mm thick, 4% blood, 70% water), and deep blood net dermis (0.3 mm thick, 10% blood, 70% water). The properties of the dominant absorbers (i.e., epidermal melanin, blood lactate, lipid, and water) and scatterers (i.e., dermal collagen and epidermal keratin) at the SWIR wavelengths were considered in the model. The geometry of the three-dimensional model is shown in Fig.1. An optical source of 0.1 mm Gaussian beam radius and a circular photodetector with an effective area of 0.13mm^2 were simulated on the surface of the skin tissue. Investigations were carried out to record the interaction profile, optical pathlength and penetration depth at certain SWIR wavelengths and three commonly used source-detector separations found in commercial spectrophotometers, i.e., 0.7mm, 1mm and 1.5mm. Ten optical wavelengths were chosen for the simulation which are: 1310nm, 1550nm, 1650nm, 1684nm, 1730nm, 1752nm, 1920nm, 2129nm, 2259nm and 2299nm. These wavelengths were selected based on a preliminary assessment of the absorbance peaks of the dominant chromophores at these regions [3] [11].

A volumetric distribution of absorbance was considered while modelling the multiple absorbers in the tissue layers. For example, the cumulative absorption coefficient (μ_{a_T}) for an i^{th} tissue layer, comprising volume fractions V_b of blood and V_w of water, at any wavelength λ is calculated according to the volumetric absorbance distribution consideration using Eq. 5:

$$\mu_{a_{T_i}}(\lambda) = V_{b_i} \cdot \mu_{a_b}(\lambda) + V_{w_i}\mu_{a_w}(\lambda) + \left[1 - \left(V_{b_i} + V_{w_i}\right)\right]\mu_{a_t}(\lambda) \quad \ldots\ldots \quad (5)$$

In the SWIR region, the dominant absorbers present in blood are lipids and other chromophores such as lactate and glucose. For simplicity, volume fractions of lipids and lactate in blood were considered as V_{lip} and V_{lact}, respectively, the cumulative blood absorption coefficient μ_{a_b} is calculated using Eq. 2:

$$\mu_{a_b}(\lambda) = V_{lact}\mu_{a_{lact}}(\lambda) + V_{lip}\mu_a(\lambda) \qquad \ldots\ldots (6)$$

In Eqs. 5 and 6, $\mu_{a_W}, \mu_{a_{lact}}, \mu_{a_{lip}}$ represent the absorption coefficients of water, lactate, and lipid, respectively. The baseline tissue absorption coefficient (i.e., tissue with no water, blood, or any other absorbers) is calculated following Eq 7:

$$\mu_{a_t}(\lambda) = 7.84 \times 10^8 \times \lambda^{-3.255} \qquad \ldots\ldots (7)$$

Simulations were carried out with a nominal volume fraction of blood lactate 2mmol/L (i.e., $V_{lact} = 36\%$) and the rest of the blood consisting of lipid and water.

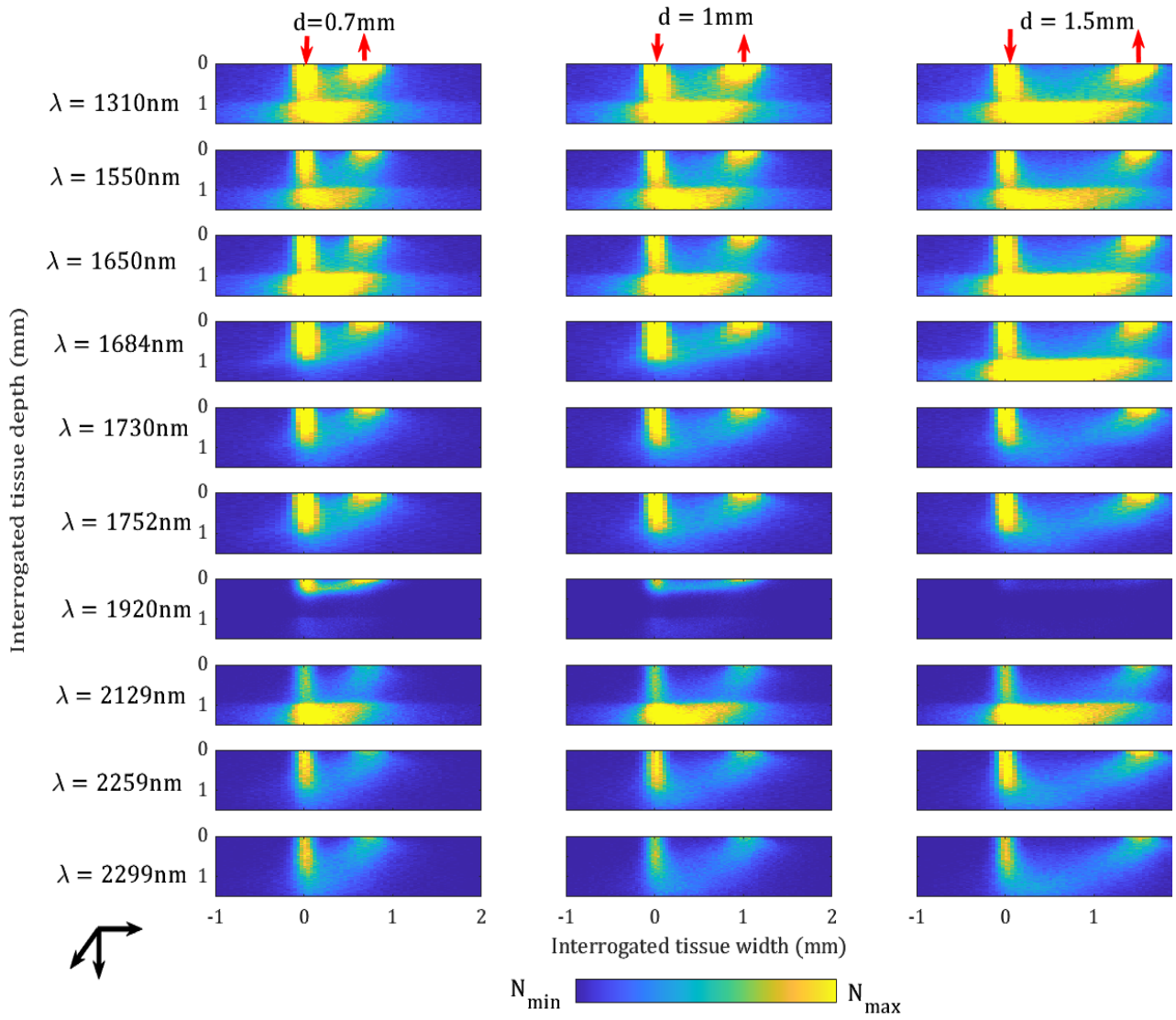

Fig.2. Light-tissue interaction profiles at SWIR wavelengths (λ) = 1310 nm,1550 nm,1650 nm,1684 nm,1730 nm,1752 nm,1920 nm,2129 nm, 2259 nm, & 2299 nm at the source-detector separations $d = 0.7\ mm$, 1 mm & 1.5 mm. The red upward and downward arrows represent the photon incidence and detection through the source and detector, respectively. The colorbar represents the distribution of the interaction events (N) between the maximum and minimum values.

III. Results and Discussion

A. *Light-tissue interaction profile*

The simulated interaction profile at the ten wavelengths and three source-detector separations are shown in Fig 2. As can be seen from Fig 2., the maximum number of interaction events (N) are visible near the source and the detector. At increasing separation distances, the spatial distribution of photons increases. At lower wavelengths, the tissue scattering coefficient is higher, resulting in higher interaction events as shown at 1310 nm, 1550 nm, and 1650 nm. With an increase in wavelength, the scattering coefficient, and therefore the number of interaction events decrease. The interaction profiles are the combined effect of the absorption properties of water, lipid, and lactate, and the Mie and Rayleigh scattering properties of smaller and larger collagen fibers, respectively. It's also worth noting that the diffusion path differs significantly from the UV/visible light interaction path, which is typically 'banana-shaped'.

B. *Mean optical pathlength and penetration depth*

The mean optical pathlength and the mean interrogated penetration depth through skin at the SWIR wavelengths at the three source-detector separations are illustrated in Fig.3. The pattern of variation of the optical pathlength and penetration depth along with the increasing SWIR wavelengths are similar, however, there is a certain noticeable mismatch especially at the wavelengths near the water absorption peaks. At all wavelengths, as expected, the highest optical pathlength and penetration depths are seen at 1mm separation distance, the lowest being 0.7mm. The variation in optical pathlength with the increasing source-detector separation is much higher

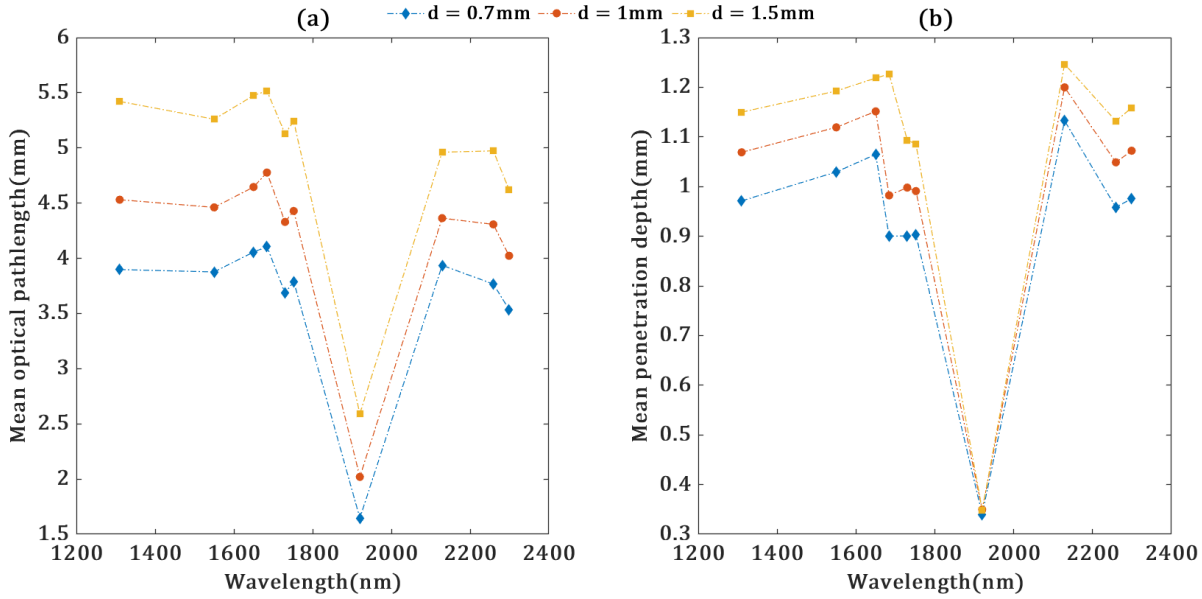

Fig. 3. SWIR distribution of mean optical pathlength (a) and penetrated depth (b) through skin.

compared to the variation in the penetration depth. In other words, at SWIR wavelengths, with the increasing source-detector separation, even though the optical pathlength varies significantly, the penetration depth does not increase as much. This is a possible reason why it is difficult to collect optical signals from tissue depths at SWIR wavelengths compared to the near-infrared wavelengths where both the optical pathlength and penetration depth change rapidly with the source-detector separation [9]. This observation can be explained by Fig.2. where with increasing source-detector separation the spatial distribution of photons increases more along the x-axis rather than z-axis. The mean penetration depth and optical path are the lowest at 1920 nm due to the high-water absorbance, which also agrees with Fig.2.

IV. Conclusion

A robust three-dimensional Monte Carlo model of light-tissue interaction has been explored at the short-wave infrared wavelengths in order to characterize the light-tissue interaction profile, optical pathlength and depth of penetration through skin for the first time. Consideration of the volumetric absorption properties of lipid, lactate, water, and melanin, and the Mie and Rayleigh scattering contribution of collagen resulted in the comprehensiveness of the model. A systematic simulation approach has revealed that the light-tissue interaction profile is different compared to the more traditional 'banana' shaped photon-path. The optical pathlength and penetration depth characterization showed the feasibility of a SWIR light to interrogate with the vascular network within the dermis and established the potential as a novel optical sensor. Information presented in the paper are invaluable to understand the light-tissue interaction at the short wave infrared optical wavelengths. Such information could contribute greatly to the design of novel optical biosensors.

References

[1] R. H. Wilson *et al*, "Review of short-wave infrared spectroscopy and imaging methods for biological tissue characterization," *J. Biomed. Opt.*, vol. 20, *(3)*, pp. 030901, 2015.

[2] S. Delbeck *et al*, "Non-invasive monitoring of blood glucose using optical methods for skin spectroscopy-opportunities and recent advances," *Anal. Bioanal Chem.*, vol. 411, *(1)*, pp. 63-77, 2019. . DOI: 10.1007/s00216-018-1395-x [doi].

[3] K. Budidha *et al*, "Identification and Quantitative Determination of Lactate Using Optical Spectroscopy—Towards a Noninvasive Tool for Early Recognition of Sepsis," *Sensors*, vol. 20, *(18)*, pp. 5402, 2020.

[4] M. Mamouei *et al*, "Comparison of wavelength selection methods for in-vitro estimation of lactate: a new unconstrained, genetic algorithm-based wavelength selection," *Scientific Reports*, vol. 10, *(1)*, pp. 1–12, 2020.

[5] T. D. Ridder *et al*, "Comparison of spectroscopically measured finger and forearm tissue ethanol concentration to blood and breath ethanol measurements," *J. Biomed. Opt.*, vol. 16, *(2)*, pp. 028003, 2011. . DOI: 10.1117/1.3535594 [doi].

[6] L. Wang, S. L. Jacques and L. Zheng, "MCML--Monte Carlo modeling of light transport in multi-layered tissues," *Comput. Methods Programs Biomed.*, vol. 47, *(2)*, pp. 131-146, 1995. . DOI: 0169-2607(95)01640-F [pii].

[7] I. V. Meglinski and S. J. Matcher, "Computer simulation of the skin reflectance spectra," *Comput. Methods Programs Biomed.*, vol. 70, *(2)*, pp. 179-186, 2003. . DOI: S0169260702000998 [pii].

[8] S. Chatterjee, K. Budidha and P. A. Kyriacou, "Investigating the origin of photoplethysmography using a multiwavelength Monte Carlo model," *Physiol. Meas.*, vol. 41, *(8)*, pp. 084001, 2020.

[9] S. Chatterjee and P. A. Kyriacou, "Monte Carlo Analysis of Optical Interactions in Reflectance and Transmittance Finger Photoplethysmography," *Sensors (Basel)*, vol. 19, *(4)*, pp. 10.3390/s19040789, 2019. . DOI: E789 [pii].

[10] S. Chatterjee *et al*, "Investigating optical path and differential pathlength factor in reflectance photoplethysmography for the assessment of perfusion," *J. Biomed. Opt.*, vol. 23, *(7)*, pp. 1-11, 2018. . DOI: 10.1117/1.JBO.23.7.075005 [doi].

[11] N. Baishya *et al*, "In-vitro spectrometric analysis of hyperlactatemia and lactic acidosis in buffer relating to sepsis," *Journal of Near Infrared Spectroscopy*, pp. 0967033520968951, 2020.